

A calcium-redox feedback loop controls human monocyte immune responses: The role of ORAI Ca²⁺ channels

Stephanie Saul,^{1*} Christine S. Gibhardt,¹ Barbara Schmidt,^{1,2,3} Annette Lis,¹ Bastian Pasiaka,¹ David Conrad,¹ Philipp Jung,⁴ Rosmarie Gaupp,⁴ Bodo Wonnberg,⁵ Ebru Diler,⁵ Hedwig Stanisz,⁶ Thomas Vogt,⁶ Eva C. Schwarz,¹ Markus Bischoff,⁴ Mathias Herrmann,⁴ Thomas Tschernig,⁵ Reinhard Kappl,¹ Heiko Rieger,² Barbara A. Niemeyer,³ Ivan Bogeski^{1†}

In phagocytes, pathogen recognition is followed by Ca²⁺ mobilization and NADPH oxidase 2 (NOX2)-mediated “oxidative burst,” which involves the rapid production of large amounts of reactive oxygen species (ROS). We showed that ORAI Ca²⁺ channels control store-operated Ca²⁺ entry, ROS production, and bacterial killing in primary human monocytes. ROS inactivate ORAI channels that lack an ORAI3 subunit. Staphylococcal infection of mice reduced the expression of the gene encoding the redox-sensitive *Orai1* and increased the expression of the gene encoding the redox-insensitive *Orai3* in the lungs or in bronchoalveolar lavages. A similar switch from ORAI1 to ORAI3 occurred in primary human monocytes exposed to bacterial peptides in culture. These alterations in ORAI1 and ORAI3 abundance shifted the channel assembly toward a more redox-insensitive configuration. Accordingly, silencing ORAI3 increased the redox sensitivity of the channel and enhanced oxidation-induced inhibition of NOX2. We generated a mathematical model that predicted additional features of the Ca²⁺-redox interplay. Our results identified the ORAI-NOX2 feedback loop as a determinant of monocyte immune responses.

INTRODUCTION

Monocytes are central effector cells of the innate immune system. As professional phagocytes, they are involved in eliminating pathogens and in activating other immune cells, such as T cells. Inflammatory monocytes are precursors of dendritic cells and macrophages, which are likewise involved in the induction of the adaptive immune response and pathogen clearance (1–3). However, monocytes are also involved in pathological conditions, such as chronic progressive diseases (cancer, hypertension, and atherosclerosis) and tissue damage (which occurs in response to acute lung injury or after ischemia and reperfusion) (4–7).

Phagocytic engulfment of invading pathogens by mononuclear phagocytes and granulocytes is a key element of the innate immune response. This process begins with binding of pathogen-associated molecular patterns and other inflammatory mediators to phagocyte surface receptors and results in phagosome formation. Activation of phagocyte receptors stimulates NADPH (reduced form of nicotinamide adenine dinucleotide phosphate) oxidase 2 (NOX2) enzymes, resulting in the production of reactive oxygen species (ROS), a process also known as “oxidative burst” (8). NOX2-generated ROS are released within the phagosome and into the extracellular space (9). Hence, the enzymatic production of ROS must be tightly regulated, enabling

oxidants to function as signaling molecules and antimicrobial agents while avoiding collateral damage of host tissue. The importance of the need for strict regulation of NOX2 activity is reflected by an activation mode that requires multiple coinciding processes, leading to the assembly of spatially separated subunits into a functional holoenzyme (9). In contrast to the activation process of NOX2, how NOX2 is disassembled and switched off is less clear.

In addition to NOX2 activation, phagocyte receptor signaling stimulates the production of inositol 1,4,5-trisphosphate (IP₃) and diacylglycerol from phosphatidylinositol 4,5-bisphosphate (PIP₂). IP₃ engages the IP₃ receptors (IP₃Rs) and triggers the release of Ca²⁺ from the endoplasmic reticulum (ER) Ca²⁺ stores. The concomitant drop in ER luminal Ca²⁺ is sensed by the ER membrane-residing stromal interaction molecules (STIM1 and STIM2). Dissociation of Ca²⁺ from STIM EF-hands leads to the formation of STIM punctae and their interaction with and activation of the ORAI channels at the plasma membrane (10–12). These STIM-gated ORAI channels are also known as Ca²⁺ release-activated Ca²⁺ (CRAC) channels and are responsible for sustained, store-operated Ca²⁺ entry (SOCE) across the plasma membrane in many nonexcitable cells (13). The CRAC channels generate a Ca²⁺ current known as *I*_{CRAC} (14). In neutrophils, STIM1 is a key molecule that recruits ER junctions to the phagosome, thereby controlling phagosomal Ca²⁺ signals, which control ROS production and phagocytosis (15–18). In contrast, STIM2 has no apparent functional role in these processes (16). In addition, ion channels of the transient receptor potential (TRP) family, such as TRPM2, TRPV2, TRPC1, TRPC3, and TRPC6, have been implicated in some stage of the phagocytosis process in neutrophils and monocyte-derived cells (MDCs) (19–21).

Calcium channel function can be regulated by redox processes. Voltage-gated Ca²⁺ channels, *N*-methyl-D-aspartate (NMDA)-type glutamate receptors, IP₃Rs, and some members of the TRP family can be regulated by oxidation (22, 23). Mammals have three isoforms of ORAI, encoded by three genes, namely *ORAI1*, *ORAI2*, and *ORAI3*. STIM1-activated ORAI1 channels

¹Department of Biophysics, Center for Integrative Physiology and Molecular Medicine (CIPPM), School of Medicine, Saarland University, Homburg 66421, Germany. ²Department of Theoretical Physics, Saarland University, Saarbrücken 66123, Germany. ³Molecular Biophysics, CIPMM, School of Medicine, Saarland University, Homburg 66421, Germany. ⁴Institute of Medical Microbiology and Hygiene, Saarland University, Homburg 66421, Germany. ⁵Department of Anatomy, School of Medicine, Saarland University, Homburg 66421, Germany. ⁶Department of Dermatology, Venereology and Allergology, University Hospital of Saarland, Homburg 66421, Germany. *Present address: Department of Cell Physiology and Metabolism, University of Geneva, 1 Rue Michel-Servet, CH-1211 Geneva, Switzerland. †Corresponding author. E-mail: ivan.bogeski@uks.eu

can be regulated by oxidative modifications of cysteine residues in both ORAI1 and STIM1 (24–27). However, in a heteromeric channel complex, inclusion of a single ORAI3 subunit, which does not have the redox-sensitive cysteine, is sufficient to render the ORAI3/ORAI1 channel redox-insensitive (28).

The physiological functions of human monocytes, MDCs, and neutrophils depend on both Ca^{2+} and redox signals (29). Therefore, these phagocytic cells represent an ideal cellular system for examining the complex interplay between Ca^{2+} and ROS. Here, we examine the functional role of ORAI and STIM in human monocytes, the functional interplay between NOX2 and ORAI/STIM Ca^{2+} channels, and the effect of varying the ratio of ORAI3 and ORAI1 on the redox sensitivity of SOCE and the crosstalk between ORAI/STIM channels and NOX2. Given the complexity of the ORAI/STIM-NOX2 interaction, we developed a theoretical model that integrates our experimental observations, provides further information, and helps in understanding the molecular mechanisms of the Ca^{2+} -redox feedback loop.

RESULTS

CRAC channels control bacterial killing in human monocytes

The formyl peptide receptors (FPRs) are G protein (heterotrimeric guanine nucleotide-binding protein)-coupled receptors (GPCRs) and are present in primary human monocytes (30, 31). To examine the role of FPRs on Ca^{2+} homeostasis, we exposed monocytes to formylated bacterial peptides, measured intracellular Ca^{2+} concentration ($[\text{Ca}^{2+}]_i$) by preloading the cells with the calcium-sensitive dye Fura-2, and measured H_2O_2 production with the peroxide-sensitive dye Amplex UltraRed, which detects extracellular H_2O_2 . Addition of the bacteria-derived peptide fMLF, which activates FPR1 and, at higher concentrations, FPR2 (30, 31), initiated a rapid increase in $[\text{Ca}^{2+}]_i$ (Fig. 1A) and a slower sustained increase in H_2O_2 (Fig. 1B).

To identify Ca^{2+} channels that may contribute to these responses, we assessed protein or transcript abundance for components of the CRAC channel and members of the TRP family in primary monocytes isolated from healthy donors. The major CRAC channel components ORAI1 and its activators STIM1 and STIM2 can be assessed by Western blotting; however, highly specific antibodies are not available for ORAI2 and ORAI3. Therefore, we measured the abundance of the transcripts for *ORAI1*, *ORAI2*, and *ORAI3* in primary human monocytes, which showed that transcripts for *ORAI1* were the most abundant (fig. S1A). Western blotting confirmed the presence of ORAI1, as well as STIM1 and STIM2 (Fig. 1C).

TRPM2 and TRPV2 are involved in chemokine secretion and phagocytosis of murine MDCs (20, 21). These channels are not controlled by STIM proteins (32). TRPC1 and TRPC6, which are regulated by STIM1, control ROS production in neutrophils (19, 33). To examine a possible contribution of TRPs in monocyte SOCE, we assessed transcript abundance for TRP family members in primary human monocytes of three healthy donors (fig. S1B). We detected transcripts encoding TRPV1, TRPV2, TRPM2, TRPM4, and TRPM7. Because the abundance of transcripts for the STIM1-regulated family members TRPC1 and TRPC6 was low or undetectable, we anticipate that these channels are unlikely to contribute to monocyte SOCE.

NOX2 is the predominant NOX isoform and a major source of ROS in MDCs and granulocytes (9). Consistent with the known role of NOX2 in mediating the oxidative burst, we confirmed that *NOX2* transcripts were the most abundant in primary human monocytes (fig. S1C).

To determine potential functions of ORAI and STIM in primary human monocytes, we knocked down ORAI1, ORAI2, ORAI3, STIM1, and

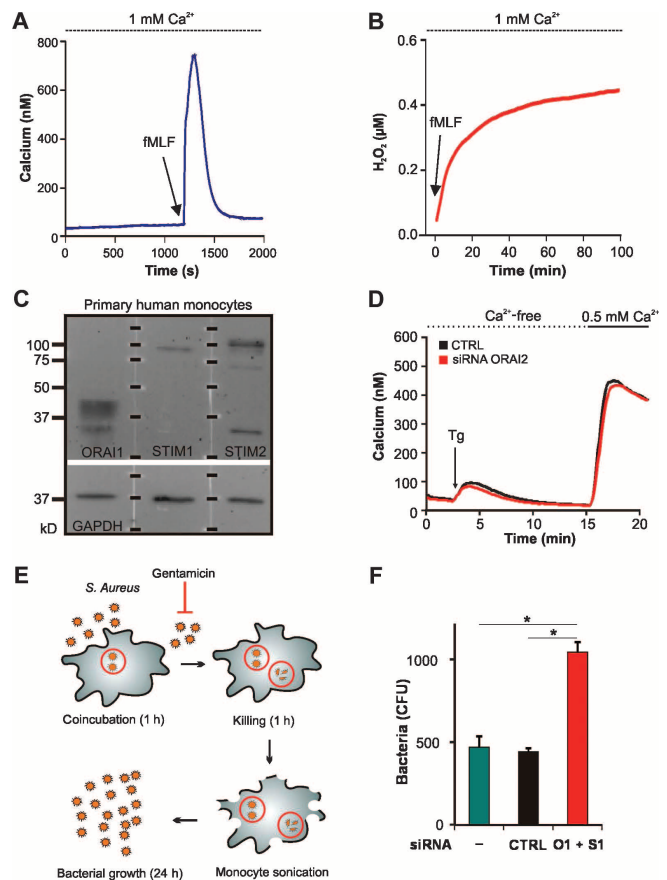


Fig. 1. ORAI and STIM control bacterial killing in primary human monocytes. (A and B) Fura-2-based imaging of $[\text{Ca}^{2+}]_i$ (A) and Amplex UltraRed measurements of H_2O_2 production by primary human monocytes after fMLF (1 μM) stimulation (B). Data are average of six experiments performed with cells from six donors. (C) Presence of ORAI1, STIM1, and STIM2 in human monocytes detected by Western blotting. Data shown are from cells from a single donor and are representative of three experiments with three donors. White lines indicate membrane sections from the same experiment incubated with different antibodies; black lines indicate marks of protein standard (kD). (D) Thapsigargin-induced SOCE in monocytes treated with control siRNA (CTRL) ($n = 571$) or siRNA against ORAI2 ($n = 925$) from eight donors. (E) Bactericidal assay schematic. (F) *S. aureus* SA113 colony-forming units (CFUs) in untransfected (–) monocytes and monocytes transfected with control siRNA or ORAI1 + STIM1 (O1 + S1) siRNAs ($n = 5$ from two healthy donors). * $P < 0.05$, using one-way analysis of variance (ANOVA) followed by Bonferroni's post hoc test (F). Data are presented as means \pm SEM.

STIM2 by small interfering RNA (siRNA) individually or in combination (fig. S2, A to C). Ca^{2+} -imaging experiments showed that ORAI2 knockdown did not impair SOCE in monocytes (Fig. 1D). Therefore, we focused on the role of ORAI1 and ORAI3 because even the presence of a single ORAI3 subunit in the heteromeric channel complex affects the redox sensitivity of the channel (28).

To assess the functional role of ORAI/STIM channels (that is, SOCE) in human monocytes, we performed a combined knockdown of ORAI1 and STIM1 and evaluated monocyte killing of *Staphylococcus aureus*

cells (Fig. 1E). ORAI1/STIM1-silenced monocytes retained a higher number of viable bacteria compared with the amounts in either of the control monocytes, indicating involvement of ORAI1 and STIM1 in the ability of monocytes to eliminate ingested pathogens (Fig. 1F).

ORAI and STIM control SOCE in human monocytes

To examine the function of ORAI1 and ORAI3 and STIM1 and STIM2 on monocyte SOCE, we stimulated the monocytes with fMLF (Fig. 2A)

or induced SOCE by depleting the ER calcium by exposing the cells to the sarco/endoplasmic reticulum Ca^{2+} -ATPase (SERCA) inhibitor thapsigargin (Fig. 2B) in the presence or absence of the nonspecific CRAC channel inhibitor 2-aminoethoxydiphenyl borate (2-APB). 2-APB impaired or abolished the calcium signal (Fig. 2, A to C). Because fMLF can stimulate other Ca^{2+} signaling events that are not mediated by SOCE, we evaluated the impact of the ORAI and STIM isoforms on monocyte SOCE induced by thapsigargin. We individually silenced ORAI1 or ORAI3, monitored

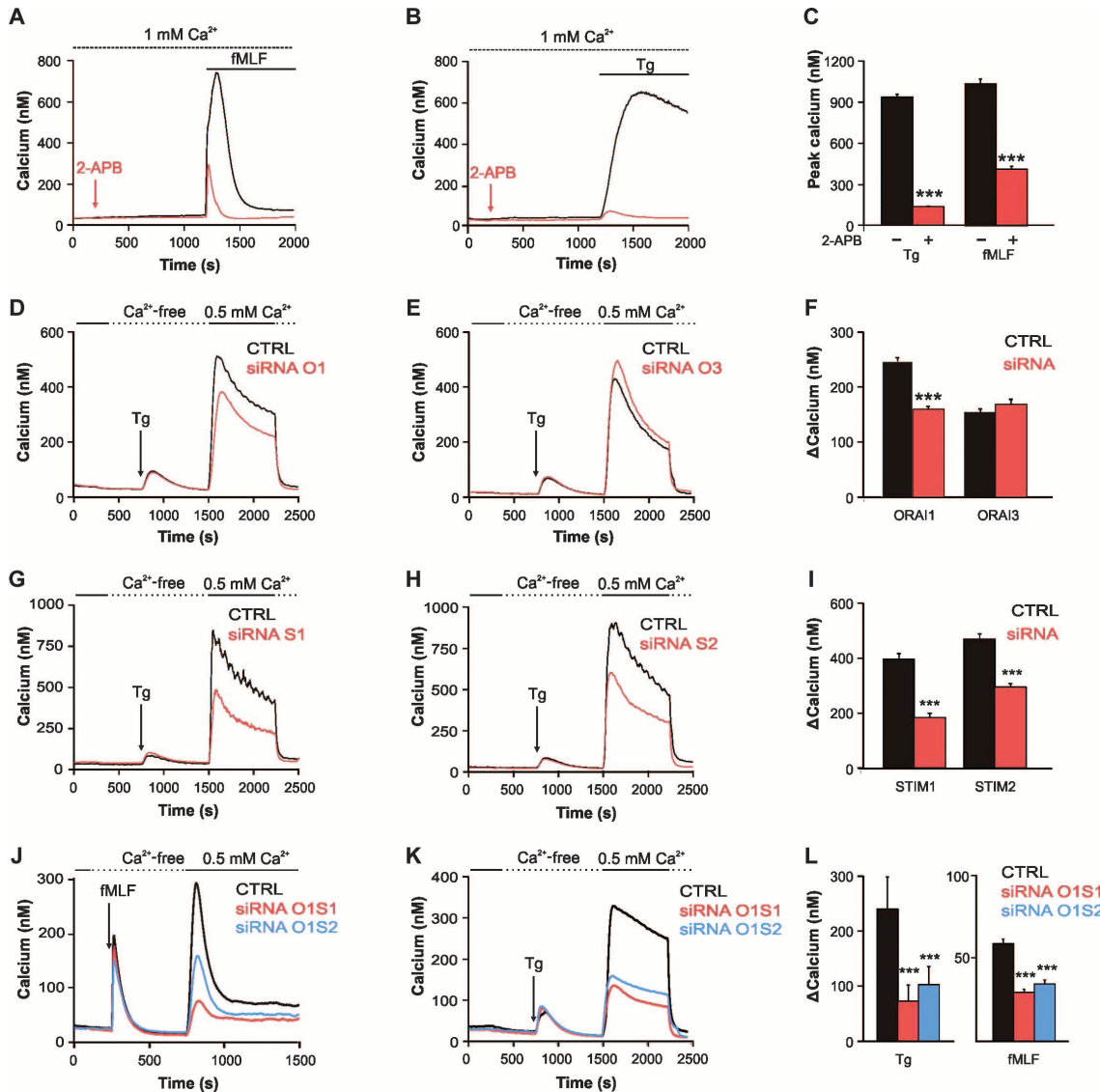


Fig. 2. ORAI and STIM control monocyte SOCE. (A and B) Fura-2-based imaging of $[Ca^{2+}]_i$ after receptor activation (A: fMLF, 1 μ M; also shown in Fig. 1A) and passive store depletion [B: thapsigargin (Tg), 1 μ M], in absence or presence of 2-APB (50 μ M). (C) Quantification of peak Ca^{2+} values for thapsigargin and fMLF treatment calculated from at least three independent experiments (donors). Cell number: $n = 690$ (thapsigargin), $n = 602$ (fMLF), $n = 606/292$ (thapsigargin \pm 2-APB), and $n = 803/714$ (fMLF \pm 2-APB). (D to L) Averaged $[Ca^{2+}]_i$ traces from thapsigargin- or fMLF-induced SOCE in mono-

cytes treated with control siRNA or siRNA, targeting ORAI1 or ORAI3 (D to F), STIM1 or STIM2 (G to I), ORAI1 + STIM1 (J to L), and ORAI1 + STIM2 (K and L). Results are presented as means, and SOCE was quantified as ΔCa^{2+} (plateau-basal). Cell number: $n = 1132/1178$ (CTRL/ORAI1), $n = 510/618$ (CTRL/ORAI3), $n = 573/580$ (CTRL/STIM1), $n = 685/711$ (CTRL/STIM2), $n = 384/483$ (CTRL/ORAI1 + STIM1), and $n = 384/461$ (CTRL/ORAI1 + STIM2). Data are presented as means \pm SEM. *** $P < 0.001$, determined by unpaired, two-sided standard Student's t test, comparing knockdown to control.

thapsigargin-induced SOCE, and quantified the Ca^{2+} signal (Fig. 2, D to F). Silencing of ORAI1 significantly reduced the Ca^{2+} signal (Fig. 2, D and F), whereas silencing of ORAI3 had no significant effect (Fig. 2, E and F). These results are consistent with the transcript abundance measurements, which indicated that ORAI1 would be more abundant than ORAI3 (assuming that transcript abundance is a suitable indication of protein abundance).

Similar measurements of SOCE in STIM1- or STIM2-silenced monocytes indicated that both STIM proteins contributed to SOCE (Fig. 2, G to I). Differences in the efficiency of knockdown (fig. S2A) may contribute to the different values obtained for the contributions of STIM1 and STIM2 to SOCE. Combined silencing of ORAI1 and STIM1 or STIM2 produced a greater inhibition of SOCE in the monocytes (Fig. 2, J to L) than did individual component silencing, both when SOCE was activated by FPR engagement (fMLF) or SERCA inhibition (thapsigargin). Silencing both STIM1 and ORAI1 was slightly more effective than silencing both STIM2 and ORAI1. In summary, these findings showed that ORAI1/STIM1 and ORAI1/STIM2 are the primary CRAC channels contributing to human monocyte Ca^{2+} homeostasis.

Monocyte oxidative burst is a Ca^{2+} -dependent process

Because Ca^{2+} and redox signaling are both important for monocyte function, we analyzed their interdependency. In neutrophils, Ca^{2+} activates the calcium-dependent protein kinase C (PKC) enzymes, such as PKC α and PKC β , which phosphorylate NOX2 component(s) and thus induce full assembly of the active holoenzyme (9, 34). We measured H_2O_2 production in human monocytes exposed to the phorbol ester PMA (phorbol 12-myristate 13-acetate) (Fig. 3A), which activates PKC enzymes without the need for Ca^{2+} , fMLF (Fig. 3B), and thapsigargin (Fig. 3C) in the presence and absence of extracellular Ca^{2+} . Exposure of human monocytes to PMA activated the oxidative burst independently of the external Ca^{2+} concentration (Fig. 3, A and D). However, the fMLF-stimulated H_2O_2 production was impaired in the absence of external Ca^{2+} (Fig. 3, B and D), which is similar to the response observed in HL-60 neutrophil-like cells (35). These results did not indicate that the remaining H_2O_2 production is Ca^{2+} -independent (for example, fMLF induces release of Ca^{2+} from the ER) but suggested that a fraction of NOX2 activity relies on Ca^{2+} entry across the plasma membrane.

Thapsigargin, which activates SOCE without activating the FPR pathway, depended on extracellular Ca^{2+} to stimulate H_2O_2 production, indicating NOX2 activation (Fig. 3, C and D). Indeed, thapsigargin-induced NOX2 activity in monocytes exhibited a linear correlation with the extracellular Ca^{2+} concentration (Fig. 3, E and F). We also confirmed the Ca^{2+} dependency of ROS production using electron paramagnetic resonance (EPR) to detect superoxide (O_2^-) production (Fig. 3, G and H).

To investigate whether ROS production requires the PKC pathway and confirm that NOX enzymes produced the measured ROS, we measured thapsigargin-induced O_2^- production from monocytes in the presence of the NOX inhibitor diphenyleioidonium (DPI) and the PKC α and PKC β inhibitor Gö6976 (Fig. 3, G and H). The presence of either inhibitor significantly impaired the oxidative burst.

Collectively, these results indicated that in human monocytes, NOX2 activity is controlled by SOCE in a manner dependent on the Ca^{2+} signal. Furthermore, the Ca^{2+} -dependent forms of PKC served as a relay between ORAI/STIM-mediated SOCE and activation of NOX2 to promote the oxidative burst.

ORAI and STIM control monocyte ROS production

On the basis of the importance of Ca^{2+} for NOX2 activity and the role of ORAI/STIM in mediating monocyte SOCE, we tested the individual con-

tribution of each CRAC channel component on monocyte H_2O_2 production. We silenced ORAI1, ORAI3, STIM1, and STIM2 individually or in combination and measured thapsigargin- or fMLF-induced H_2O_2 production (Fig. 4 and fig. S3). Silencing ORAI1 significantly inhibited H_2O_2 production (Fig. 4A and fig. S3A), whereas ORAI3-silenced monocytes tended toward generating more H_2O_2 (Fig. 4B and fig. S3B). Moreover, knocking down STIM1 or STIM2 inhibited thapsigargin-induced H_2O_2 production (Fig. 4, C and D), and, similar to the results of STIM knockdown on SOCE (Fig. 2), STIM1 knockdown had a stronger effect than STIM2 knockdown. STIM knockdown produced a greater reduction in H_2O_2 production than reduction in SOCE (compare Fig. 2I and Fig. 4, C and D), suggesting that STIM proteins may have SOCE-independent effects on NOX2. For example, STIM may promote NOX2 assembly. Combined silencing of ORAI1 and STIM1 or STIM2 almost fully abrogated or strongly reduced NOX2 activity, respectively (Fig. 4E). Combined STIM1 and STIM2 silencing also reduced H_2O_2 production in monocytes exposed to fMLF (fig. S3C).

The data presented in Fig. 4 are from several experiments performed with cells obtained from different human donors. For simplicity, we averaged all values, calculated the SEMs, and determined significance (*t* test) at different time points. However, we observed a strong donor dependence with regard to H_2O_2 production, which complicates the statistical analysis between control and ORAI/STIM-silenced cells. Hence, we used an alternative analysis approach to confirm the significant differences in H_2O_2 production between control and ORAI/STIM-silenced monocytes (fig. S4, A to C). We also confirmed that knocking down ORAI1, STIM1, and STIM2 together or ORAI3 in the monocytes did not compromise phagocytosis of uncoated latex beads (fig. S5, A to C), indicating that the effect of ORAI/STIM on H_2O_2 production was specific and that not all Ca^{2+} -dependent processes required ORAI/STIM-mediated SOCE.

The ratio of ORAI3 to ORAI1 controls redox sensitivity of monocyte SOCE and is increased upon bacterial infection

Our data showed that ORAI/STIM channels regulate monocyte Ca^{2+} homeostasis and that ORAI/STIM-mediated SOCE stimulated NOX2 activity. However, ORAI/STIM channels are redox-regulated with the presence of a single ORAI3 subunit sufficient to render an ORAI3/ORAI1 heteromeric channel redox-insensitive, whereas channel complexes lacking ORAI3 are inhibited by oxidation (28). Accordingly, the relative ORAI3/ORAI1 abundance ratios are functionally more relevant than the absolute amount of the individual isoforms. Hence, we calculated the ORAI3 to ORAI1 relative expression ratios from the transcript analysis (fig. S2A) and compared them with the ratio of ORAI3/ORAI1 in naïve and effector human T cells (Fig. 5A) using the data from (24) for the naïve and effector human T cell transcript abundance. The ORAI3/ORAI1 ratio was highest in monocytes, which we expected because NOX2 is abundant in monocytes and some activity occurs even under nonpathogenic conditions. Thus, compared to T cells, monocytes likely experience more oxidative stress, thereby needing a higher ORAI3/ORAI1 ratio.

To test for a role of ORAI3 in the sensitivity of monocyte SOCE to oxidative stress, we exposed human monocytes to different concentrations of H_2O_2 for 15 min, a sufficient time for oxidation of the channel to occur, and measured thapsigargin-induced Ca^{2+} entry (Fig. 5B). As the H_2O_2 concentration increased, the amplitude of the peak of the Ca^{2+} increase decreased with an IC_{50} (median inhibitory concentration) value for H_2O_2 of ~155 μM (Fig. 5C). This monocyte IC_{50} , which was calculated using a second-degree exponential decay fit, was significantly higher than those for CD4⁺ effector (83.4 μM) and naïve T cells (10.3 μM) (24). Moreover,

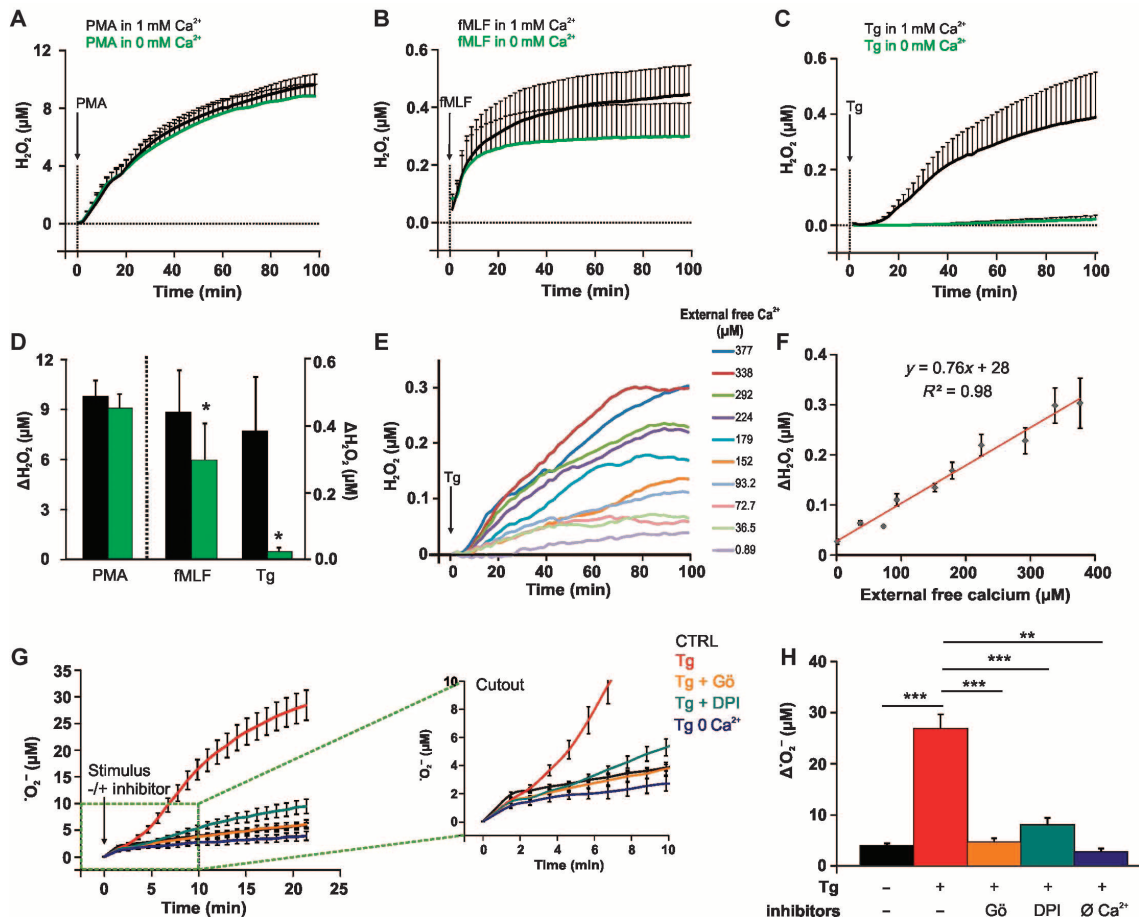


Fig. 3. Ca²⁺ dependence of NOX2-mediated ROS production in monocytes. Time-resolved Amplex Red-based measurements of H₂O₂ production by primary human monocytes in the presence or absence of extracellular Ca²⁺. (A) Activation through PKC by addition of PMA (1 μM). (B) Activation by fMLF (1 μM) stimulating its receptor activation. (C) Activation by passive ER Ca²⁺ store depletion from thapsigargin (1 μM). (D) Quantification of H₂O₂ concentration from data shown in (A) to (C) after 90 min. (E) Dependence of monocyte H₂O₂ production on external Ca²⁺. (F) Correlation between H₂O₂ production (quantified as ΔH₂O₂) and extracellular Ca²⁺

concentration. (G) Time-resolved EPR-based measurements of thapsigargin-induced *O₂⁻ production. The exact conditions are indicated in the “cut-out.” (H) Quantification of Δ*O₂⁻ from data shown in (G). $n = 14$ (CTRL), $n = 6$ (thapsigargin), and $n = 4$ [Gö6976 (Gö), DPI, and Ca²⁺-free] independent experiments (where n is the number of donors tested). Data are presented as means ± SEM. In (D), results in the presence and absence of Ca²⁺ are compared. In (H), the indicated pairs were assessed by unpaired, two-sided standard Student’s t test (* $P < 0.05$, ** $P < 0.01$, and *** $P < 0.001$).

there was a correlation between the ratio of *ORAI3/ORAI1* transcript and the sensitivity of SOCE to H₂O₂, indicating that as the amount of ORAI3 increased in the cells, redox sensitivity decreased (Fig. 5D). To establish the role of ORAI3 in limiting SOCE redox sensitivity, we evaluated the amount of H₂O₂-induced SOCE inhibition in control and ORAI3-silenced monocytes (Fig. 5, E to G). Silencing ORAI3 caused a small but significant increase in SOCE and a significant increase in the inhibition of SOCE by H₂O₂, indicating an increase in redox sensitivity of the channel (Fig. 5G).

Because we observed that monocytes had a higher *ORAI3/ORAI1* ratio than T cells, we postulated that this may relate to their exposure to oxidative stress in the donors. To test this hypothesis, we exposed primary human monocytes to fMLF or the phorbol ester PMA and measured the abundance of *ORAI1* and *ORAI3* transcripts (Fig. 5, H, I, and K, and fig. S6, A and B)

and calculated the *ORAI3/ORAI1* ratio (Fig. 5J and fig. S6C). Both stimuli induce NOX2 activation and ROS production (Fig. 3, A and B); however, fMLF depended on extracellular Ca²⁺, but PMA did not. After 24 hours, monocytes exposed to fMLF exhibited reduced *ORAI1* and increased *ORAI3* transcripts (Fig. 5, H and I), thereby resulting in about twofold increase in *ORAI3/ORAI1* ratio over that in the unstimulated or 4 hour-stimulated cells (Fig. 5, J and K). Furthermore, PMA also reduced *ORAI1* and increased *ORAI3* transcripts with effects detectable 4 hours after stimulation and persisting 24 hours after stimulation (fig. S6).

To study whether this switch in ORAI subunits occurs in vivo, we exposed C57BL/6 mice to *S. aureus* to cause an acute lung infection. Six hours after the bacterial challenge, we euthanized the mice and collected bronchoalveolar lavage fluids (BALFs) to obtain mostly monocytes and lung tissues for transcript analyses. We confirmed infection by determining

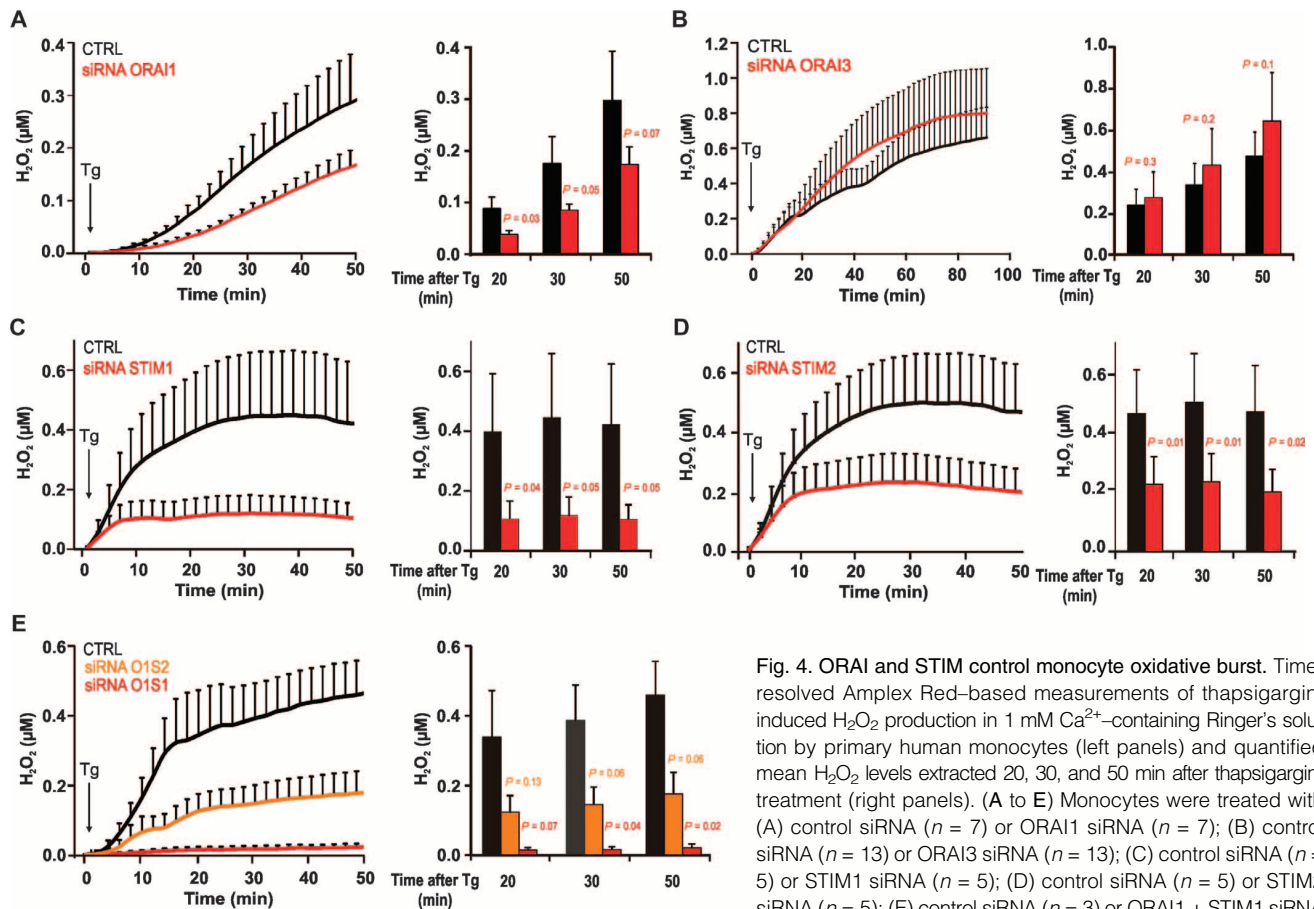


Fig. 4. ORAI and STIM control monocyte oxidative burst. Time-resolved Amplex Red-based measurements of thapsigargin-induced H_2O_2 production in 1 mM Ca^{2+} -containing Ringer's solution by primary human monocytes (left panels) and quantified mean H_2O_2 levels extracted 20, 30, and 50 min after thapsigargin-treatment (right panels). (A to E) Monocytes were treated with (A) control siRNA ($n = 7$) or ORAI1 siRNA ($n = 7$); (B) control siRNA ($n = 13$) or ORAI3 siRNA ($n = 13$); (C) control siRNA ($n = 5$) or STIM1 siRNA ($n = 5$); (D) control siRNA ($n = 5$) or STIM2 siRNA ($n = 5$); (E) control siRNA ($n = 3$) or ORAI1 + STIM1 siRNA

($n = 3$) or ORAI1 + STIM2 siRNA ($n = 3$). Data are presented as means \pm SEM, and P values are indicated as determined by paired, two-sided standard Student's t test.

the bacterial loads in the BALFs and lung homogenates (fig. S7, A and B), and we confirmed recruitment of immune cells to the lungs (fig. S7C). Similar to the switch in ORAI subunits that we observed for the primary human monocytes, *Orai1* transcripts decreased and *Orai3* transcripts increased, resulting in an increase in the *Orai3/Orai1* ratio in both the BALFs (Fig. 5, L to N) and lung tissues (Fig. 5, O to Q). Different than the results with the human monocytes exposed to fMLF, the increase in the *Orai3/Orai1* ratio in the mice resulted from a more pronounced decrease in *Orai1* than an increase in *Orai3* transcripts (Fig. 5, L, M, O, and P). These findings suggested that, in rodents, *Orai1* down-regulation might be a more important protective mechanism against oxidative stress and inflammation than the up-regulation of *Orai3*, which we observed in the human monocytes in culture.

ORAI and NOX2 form a feedback loop

Our findings suggested that a feedback loop exists between Ca^{2+} (ORAI/STIM) and ROS (NOX2). Evaluating the physiological significance of the feedback loop in vivo or in cells is difficult because ORAI1 or STIM deficiency will impair SOCE and thus decrease NOX2 activity and ROS production, eliminating the feedback loop from NOX2 to ORAI/STIM. Similarly, NOX2 deficiency blocks ROS production, also preventing any signaling from NOX2 to ORAI/STIM channels. However, we reasoned that we could compare the SOCE-mediated ROS

production in control monocytes and ORAI3 knockdown cells that had been pre-exposed to oxidative conditions (H_2O_2), then washed and loaded with a ROS-sensitive dye, and then exposed to thapsigargin to stimulate SOCE-mediated ROS production (Fig. 6A). We set the thapsigargin-induced ROS signal in untransfected monocytes that had not been exposed to H_2O_2 as the maximal (100%) response (Fig. 6B). Control siRNA-transfected monocytes exhibited little redox-mediated inactivation of the SOCE-induced ROS signal, whereas monocytes in which ORAI3 was knocked down exhibited $\sim 20\%$ inhibition of the thapsigargin-induced ROS production (Fig. 6C). These data suggested that human monocytes that are not under oxidative stress have sufficient ORAI3 to render most of the ORAI/STIM complexes insensitive to redox-mediated inactivation and confirmed a regulatory role for ORAI3 in the ORAI/STIM-NOX2 feedback loop.

A mathematical model predicts additional features of the ORAI-NOX2 feedback loop

Our experiments showed that a low *Orai3/Orai1* expression ratio means not only greater SOCE but also greater CRAC channel redox sensitivity, yet greater SOCE should produce greater NOX2 activity and increased ROS production. The interdependence of NOX2 (ROS signals) and ORAI/STIM channels (Ca^{2+} signals) is complex and determined by several variables that cannot be easily measured. Therefore, we developed a theoretical

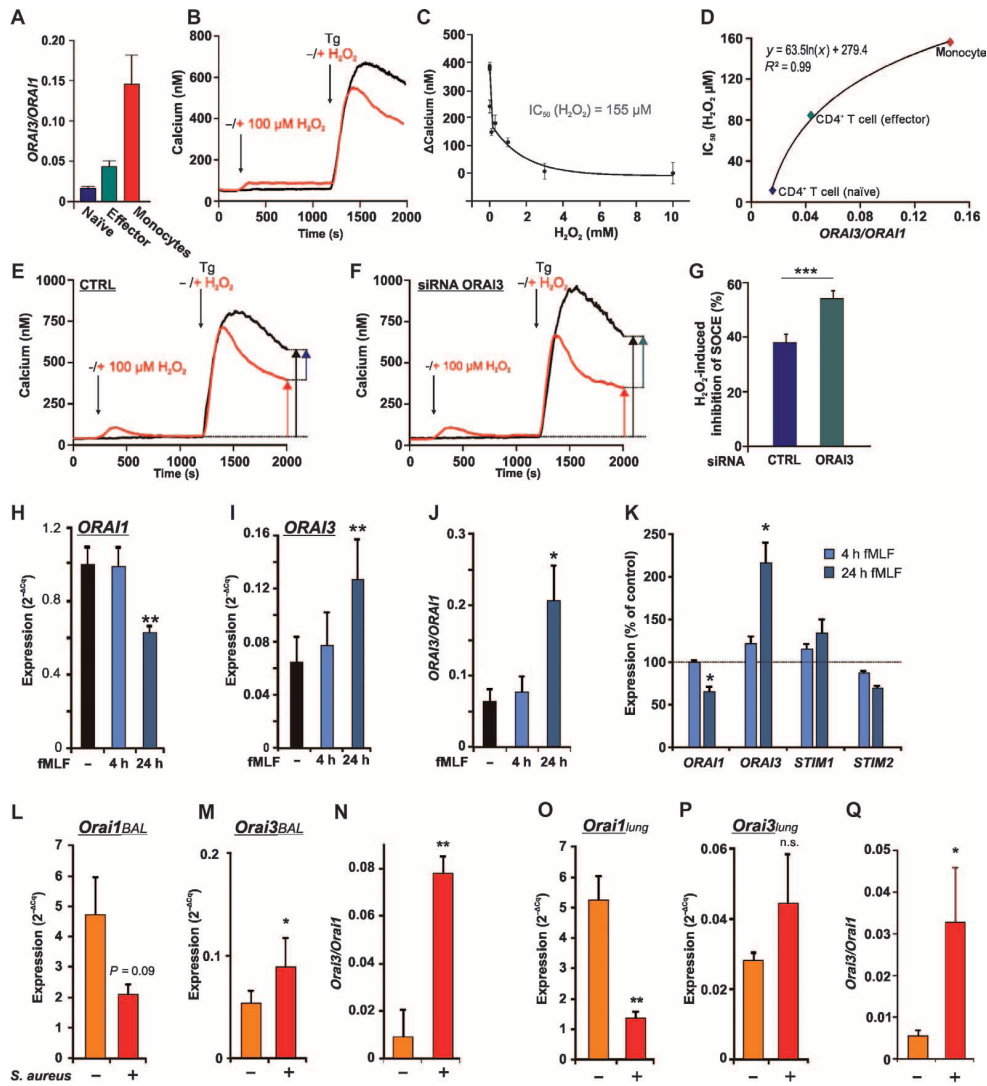


Fig. 5. Redox sensitivity of monocyte SOCE is modulated by ORAI3/ORAI1 ratio. (A) Quantitative reverse transcription polymerase chain reaction (qRT-PCR) quantified *ORAI3/ORAI1* ratios in human T cells and monocytes. (B) Fura-2-based imaging of $[Ca^{2+}]_i$ in thapsigargin-treated human monocytes in the absence or presence of 100 μ M H_2O_2 . (C) Dependence of $\Delta[Ca^{2+}]_i$ (plateau-basal) on external H_2O_2 after thapsigargin stimulation in human monocytes. IC_{50} value was determined on the basis of a second-order exponential decay fit of the data. Kinetics and quantifications were averaged from $n = 606$ (no H_2O_2), $n = 832$ (1 μ M H_2O_2), $n = 382$ (10 μ M), $n = 420$ (100 μ M), $n = 101$ (300 μ M), $n = 499$ (1 mM), $n = 111$ (3 mM), and $n = 394$ (10 mM) cells. (D) Correlation between SOCE redox sensitivity (H_2O_2 IC_{50}) and the relative *ORAI3/ORAI1* mRNA levels in primary human naïve and effector T cells and primary human monocytes. Parameter correlation fitted by logarithmic function shown with indicated stability index. (E and F) $[Ca^{2+}]_i$ in thapsigargin-treated human monocytes transfected with control siRNA (E) or ORAI3 siRNA (F) in the absence or presence of 100 μ M H_2O_2 . (G) Quantification of data shown in (E) and (F) (indicated with arrows) as percent of inhibition of $\Delta[Ca^{2+}]_i$. SOCE from cells in the absence of H_2O_2 was calculated as 100%. Cell number: $n = 455$ (CTRL siRNA), $n = 496$ (CTRL

siRNA, H_2O_2), $n = 589$ (ORAI3 siRNA), and $n = 441$ (ORAI3 siRNA, H_2O_2). (H and I) qRT-PCR quantification of *ORAI1* and *ORAI3* transcripts in human monocytes treated with 1 μ M fMLF for 4 and 24 hours from five donors. (J) *ORAI3/ORAI1* ratios calculated from the data shown in (H) and (I). (K) Normalized expression of *ORAI1* and *ORAI3* and *STIM1* and *STIM2* against untreated control from monocytes treated with 1 μ M fMLF for 4 and 24 hours. (L and M) qRT-PCR quantification of *Orai1* and *Orai3* transcripts in BAL fluids from mock and *S. aureus* SA564-infected C57BL/6 mice ($n = 5$). (N) *Orai3/Orai1* ratios calculated from the data shown in (L) and (M). (O and P) qRT-PCR quantification of *Orai1* and *Orai3* transcripts in lungs from mock and infected ($n = 6$) mice. (Q) *Orai3/Orai1* ratios calculated from the data shown in (O) and (P). Data are presented as means \pm SEM. In (H) to (J), comparison between untreated control and 24 hours after fMLF exposure was assessed by paired, two-sided standard Student's *t* test. In (K), differences compared to the normalized untreated control were assessed by paired, two-sided standard Student's *t* test. In (G), the data were evaluated by unpaired two-sided standard student *t* test. In (L) to (Q), the indicated pairs were assessed by paired, two-sided standard Student's *t* test. n.s., nonsignificant; * $P < 0.05$, ** $P < 0.01$, and *** $P < 0.001$.

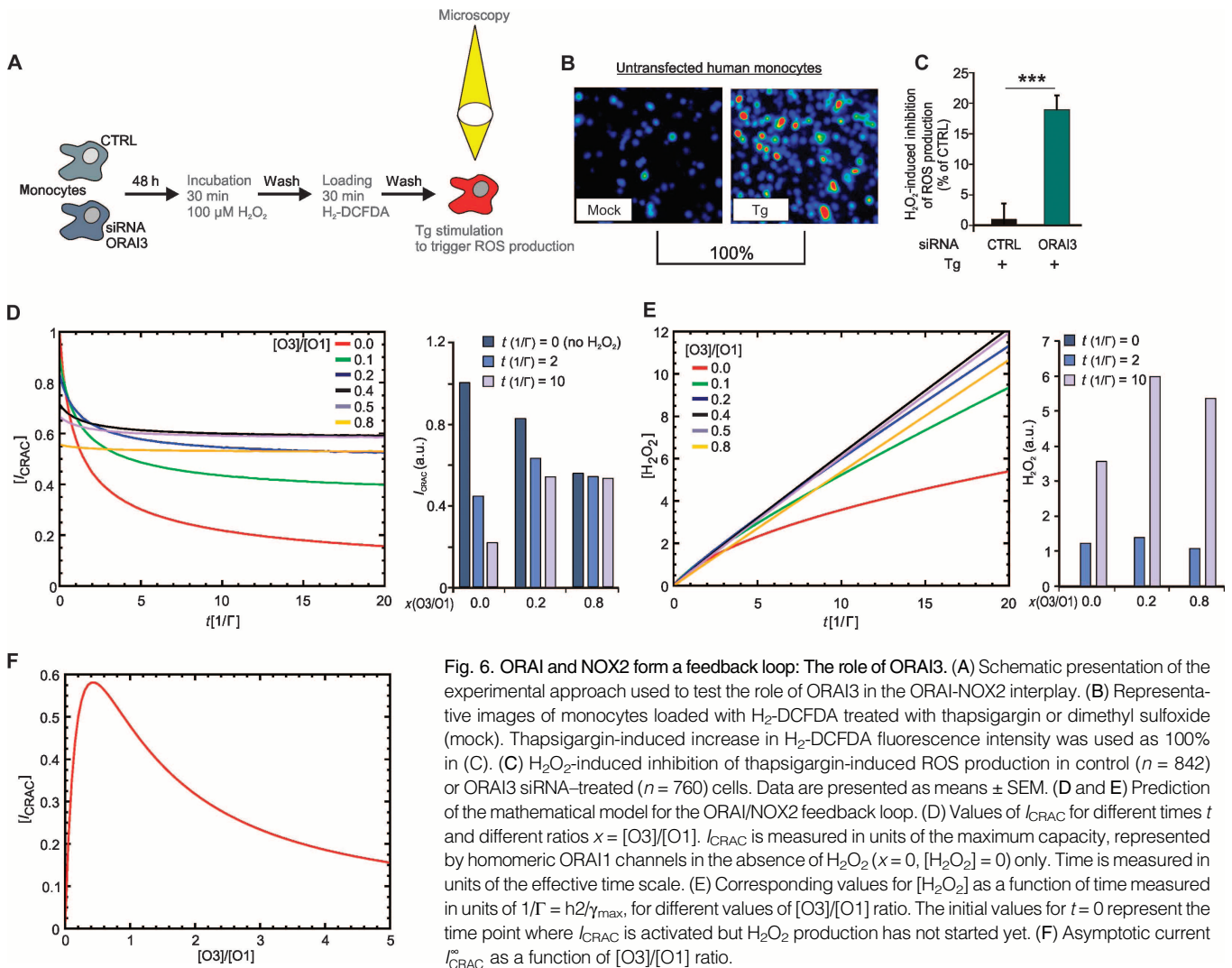


Fig. 6. ORAI and NOX2 form a feedback loop: The role of ORAI3. (A) Schematic presentation of the experimental approach used to test the role of ORAI3 in the ORAI-NOX2 interplay. (B) Representative images of monocytes loaded with H₂-DCFDA treated with thapsigargin or dimethyl sulfoxide (mock). Thapsigargin-induced increase in H₂-DCFDA fluorescence intensity was used as 100% in (C). (C) H₂O₂-induced inhibition of thapsigargin-induced ROS production in control ($n = 842$) or ORAI3 siRNA-treated ($n = 760$) cells. Data are presented as means \pm SEM. (D and E) Prediction of the mathematical model for the ORAI/NOX2 feedback loop. (D) Values of I_{CRAC} for different times t and different ratios $x = [O3]/[O1]$. I_{CRAC} is measured in units of the maximum capacity, represented by homomeric ORAI1 channels in the absence of H₂O₂ ($x = 0$, $[H_2O_2] = 0$) only. Time is measured in units of the effective time scale. (E) Corresponding values for $[H_2O_2]$ as a function of time measured in units of $1/\Gamma = h_2/\gamma_{max}$, for different values of $[O3]/[O1]$ ratio. The initial values for $t = 0$ represent the time point where I_{CRAC} is activated but H₂O₂ production has not started yet. (F) Asymptotic current I_{CRAC} as a function of $[O3]/[O1]$ ratio.

model to explore the dependence of SOCE (represented as I_{CRAC}) on the ratio of ORAI3/ORAI1 ($x = [O3]/[O1]$) and the concentration of H₂O₂ ($[H_2O_2]$) (see text S1 for a description of the model).

The model considers a population of monocytes (any cells with high amounts of NOX2, such as phagocytes) in a given volume of an inflamed tissue. All monocytes are assumed to have the same ORAI3/ORAI1 ratio x , be exposed to a common average external H₂O₂ concentration, and experience the same stimulus (pathogens) that triggers SOCE and, concomitantly, I_{CRAC} . The model assumes that a longer-lasting stimulus results in intermittent SOCE, leading to repeated assembly and disassembly of the CRAC channels in each individual monocyte. During each CRAC channel reassembly, the incorporation of a redox-sensitive ORAI1, redox-insensitive ORAI3, or a mixture of the two leads to an adaption of I_{CRAC} to the current external H₂O₂ concentration, resulting in an overall dependence of the average I_{CRAC} of all monocytes at a certain time t on the external H₂O₂ concentration at that time. The monocytes produce H₂O₂ when the intracellular Ca²⁺ concentration is increased after SOCE activation. Thus, a feedback loop is established between the CRAC channels (average I_{CRAC} from the whole monocyte population) and the external H₂O₂ concentration.

To quantify the feedback loop, we formulated a mathematical model for the relation between the average I_{CRAC} at time t after the SOCE-inducing stimulus and the external $[H_2O_2]$ at the same time t . We assumed that the I_{CRAC} amplitude of a hexameric CRAC channel depends on the number of ORAI3 subunits in the CRAC channel configuration and that channels without an ORAI3 (ORAI1 homomeric channels) have an additional dependence on $[H_2O_2]$. We made the following assumptions in the model: (i) for a given ORAI3/ORAI1 ratio x , the formation of CRAC channels with $n = 0, 1, \dots, 6$ ORAI3 subunits is random and noncooperative and only depends on x ; (ii) the average I_{CRAC} is the sum of seven CRAC currents corresponding to the seven possible CRAC channel configurations, each weighed with its respective probability (depending on x); (iii) the dependence of the maximum I_{CRAC} of the ORAI1 homomeric channel on $[H_2O_2]$ is sigmoidal, with the maximum at $[H_2O_2] = 0$ and approaching zero for large values of $[H_2O_2]$; (iv) the production rate of H₂O₂ is proportional to the average I_{CRAC} current.

In the absence of H₂O₂, I_{CRAC} decreases monotonically with an increasing number of ORAI3 subunits (Fig. 6D). Under these conditions ($[H_2O_2] = 0$), the redox-sensitive ORAI1 homomeric channel produces

a maximal I_{CRAC} . With increasing H_2O_2 concentration, the ORAI1 homomeric channels become oxidized and inhibited. Consistent with this observation, the model predicted that their activity is diminished, resulting in an average I_{CRAC} that decreases monotonically with time (Fig. 6D). Another prediction of the model is that, for large values of x , monocyte I_{CRAC} would be nearly constant over time because few redox-sensitive ORAI1 homomeric channels would be present at the relatively high ORAI3/ORAI1 ratio (Fig. 6D). Finally, the model also predicted that the maximal oxidative burst (maximal amount of H_2O_2 produced over time) (Fig. 6E) and I_{CRAC} (Fig. 6F) would occur when the ratio of ORAI3/ORAI1 is ~ 0.4 .

DISCUSSION

NOX2 activity both at the plasma membrane and at the phagosomes is controlled by Ca^{2+} (9, 29, 35–37). Most studies on the relationship among Ca^{2+} , NOX2, and phagocytosis have been performed in human and murine neutrophils and immortalized cell lines. However, the molecular players and the regulatory mechanisms responsible for Ca^{2+} control of NOX2 activity and vice versa are not well understood, especially in monocytes. Moreover, variations in NOX2 activation mechanisms and CRAC channel composition between different human phagocytic cells are plausible but remain to be investigated.

Here, we showed that, in primary human monocytes, bacterial peptides engage phagocyte FPRs and activate SOCE, a functionally important signaling cascade supported by a previous study showing that monocyte FPRs recognize bacterial signal peptides (30). Furthermore, we identified ORAI/STIM channels as a major Ca^{2+} -entry pathway in human monocytes and also showed that, in addition to ORAI1 and STIM1, STIM2 and ORAI3 are also important determinants of monocyte SOCE- and NOX2-dependent ROS production. Quantification of H_2O_2 and $^{\bullet}O_2^-$ production confirmed that PKC activation by PMA stimulated NOX2 through a process that was independent of extracellular Ca^{2+} , in agreement with most previous reports (9, 36). However, under physiological conditions, NOX2 depends on Ca^{2+} entry across the plasma membrane, as we have shown with the monocyte ROS response to fMLF. Accordingly, monocytes exposed to thapsigargin under Ca^{2+} -free conditions lacked ROS production, indicating absence of NOX2 activity, thus further supporting the functional importance of ORAI/STIM in stimulating the monocyte oxidative burst.

As direct measures of the functional role of ORAI/STIM in human monocytes, we measured bacterial killing and phagocytosis of uncoated beads in *ORAI/STIM*-silenced or 2-APB-treated monocytes. This analysis showed that only bacterial killing depended on ORAI/STIM. Because loss of ORAI/STIM function did not impair phagocytosis of uncoated beads but reduced elimination of *S. aureus*, these results are consistent with defective SOCE-dependent ROS production as a likely cause for the reduced bacterial killing.

Our data indicated that a high ORAI3/ORAI1 ratio suppressed SOCE amplitudes while also rendering ORAI/STIM channels less inhibited by oxidation. Examination of the isoform-specific *ORAI* expression dynamics in vitro and in vivo indicated that this ratio was physiologically important. Indeed, bacterial peptides increased in the *ORAI3/ORAI1* transcript ratio in human monocytes, and acute lung infection of mice with *S. aureus* produced a similar change in BALFs and lungs. In human monocytes, the increase in this ratio resulted from an increase in *ORAI3* transcripts, which we have also observed in T cells (24), and a decrease in *ORAI1* transcripts. In contrast, in mice, reduced *Orai1* transcripts were the main contributor to the observed increase of the *Orai3/Orai1* ratio. Thus, both *ORAI3* up-regulation and *ORAI1* down-regulation may protect monocytes from oxidative stress and limit inflammation.

On the basis of our SOCE and ROS measurements, we hypothesize that this increased ORAI3/ORAI1 ratio will cause, on one hand, a smaller but prolonged monocyte SOCE and, on the other hand, a diminished but more persistent NOX2-dependent ROS production. However, these possibilities are difficult to test experimentally. Hence, we established a mathematical model to explore the consequences of the ORAI/STIM-NOX2 feedback loop. The model generated several predictions. I_{CRAC} -induced NOX2-dependent H_2O_2 production would increase with time with a production rate that decreases with time. Under oxidative stress, I_{CRAC} would decrease with time, ultimately reaching a value determined by the CRAC channels that contain at least a single ORAI3. The steady-state value of I_{CRAC} would be zero when ORAI3 is low, would be maximal at an intermediate amount of ORAI3, and would approach the I_{CRAC} value for ORAI3 homomeric channels at high amounts of ORAI3 (fig. S6C). When ORAI3 abundance is low, the time dependence of I_{CRAC} would be strong, whereas when ORAI3 abundance is high, I_{CRAC} would be constant over time. The time at which I_{CRAC} reaches the steady-state value would be set by the inverse rate of relative maximal H_2O_2 production. The optimal ORAI3/ORAI1 ratio for monocyte function (maximal ROS production and I_{CRAC}) under oxidative stress would be ~ 0.4 . Thus, high H_2O_2 production rates or high H_2O_2 sensitivity of the ORAI1 homomeric channels would lead to I_{CRAC} rapidly reaching its stationary value. The key prediction is that changes in the expression levels of *ORAI3* and *ORAI1* would alter the ratio of these two subunits, thereby altering the amount of negative feedback from NOX2-produced ROS on the Ca^{2+} signals mediated by ORAI/STIM channels and thus producing different magnitudes and time dependencies of I_{CRAC} .

In summary, we propose a model for the interconnectivity between ORAI/STIM and NOX2 and the immune cell specificity of this regulatory network (Fig. 7). Whereas T cells have predominantly few ORAI3 subunits and thus few channels that resist oxidation-mediated inactivation, monocytes, which are responsible for producing the oxidative burst and thus experience oxidative stress, have a higher ratio of ORAI3/ORAI1 subunits, thereby optimizing SOCE and resistance to redox-mediated inhibition (Fig. 7A).

In monocytes, exposure to bacterial peptides or infection with pathogens engages phagocyte FPRs and other GPCRs to stimulate an increase in intracellular Ca^{2+} and induce SOCE. The amplitude of SOCE controls the rate of NOX2-facilitated electron transport from the cytosolic NADPH across membranes to molecular oxygen, which in turn linearly correlates with the amounts of $^{\bullet}O_2^-$ and H_2O_2 produced in the extracellular space. Thus, in inflamed tissues, the concentrations of ROS can become very high. ROS contribute to pathogen elimination and host defense but also cause collateral damage by oxidizing host cellular components. Therefore, ROS production must be tightly controlled during the innate immune response. Our data and model indicated that monocytes can optimize the ROS response by altering the ratio of ORAI3/ORAI1 and thereby tune the negative feedback from NOX2 to the ORAI/STIM channel (Fig. 7B).

Excessive innate immune responses and enhanced oxidative burst cause collateral tissue damage and even death in several human diseases (3–5, 7), whereas NOX2 deficiency leads to chronic granulomatous disease, which results from defective pathogen clearance (9, 38). Immunodeficient patients with mutations in ORAI1 and STIM1 suffer from acute bacterial sepsis (39, 40), but no studies have evaluated the role of monocytes and MDCs to the immune deficiency of these individuals. Understanding this regulatory network suggests that pharmacological tuning of ORAI/STIM-mediated SOCE could be a potential strategy to enhance innate immunity or prevent oxidant-induced collateral tissue damage.

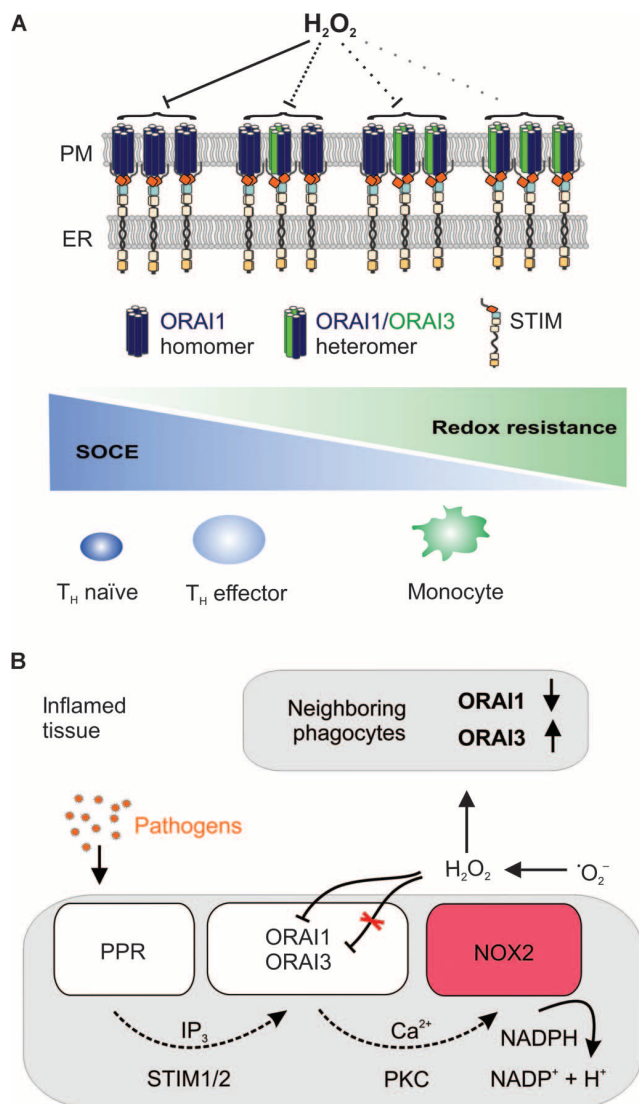


Fig. 7. Phagocyte adaptation to oxidative environments. (A) ROS inhibit ORAI1/STIM1 channels, the conductance and redox sensitivity of which depend on the ORAI3/ORAI1 ratio. Higher ORAI3/ORAI1 ratios dampen SOCE but decrease redox sensitivity. The predicted relative ORAI3/ORAI1 ratio, SOCE, and redox resistance in the indicated immune cells along the spectrum are shown. PM, plasma membrane. (B) Pathogens engage pathogen recognition receptors (PPR) and induce activation of SOCE by promoting IP₃-mediated Ca²⁺ release from the ER and activation of STIM1 and STIM2. The concomitant increase in intracellular Ca²⁺ activates NOX2 in a PKC-dependent manner, thereby initiating production of [•]O₂⁻ and subsequently H₂O₂. These ROS can act in an autocrine and in a paracrine fashion to inhibit ORAI1 in a short-term effect, but ROS also lead to a shift in the ORAI3/ORAI1 ratio, likely providing prolonged but moderate Ca²⁺-dependent ROS production in phagocytes after infection. This self-regulation of phagocyte ROS production might be essential to avoid collateral tissue damage in sites of inflammation.

MATERIALS AND METHODS

Chemicals

All chemicals, if not further indicated, were purchased from Sigma. For transfection, the Amaxa Human Monocyte Nucleofector Kit (VPA-1007) and Amaxa P3 Primary Cell 4D-Nucleofector X Kit L (V4XP-3024) were used (Lonza).

Isolation and cultivation of primary human monocytes

Research carried out for this study with human material has been approved by the local ethics committee (Unbedenklichkeitserklärung, 10.07.14; 184/02; 89/99). Primary human monocytes were isolated from peripheral blood mononuclear cells (PBMCs). PBMCs were obtained from leukocyte-reducing system (LRS) chambers, provided by the local blood bank. The cells were separated from the rest of the blood content by a standard density gradient centrifugation. Monocytes were isolated [in phosphate-buffered saline (PBS) + 0.5% bovine serum albumin] either by negative isolation or by adhesion. Negative isolation was performed using the Dynabeads Untouched Human Monocytes System following the manufacturer's instructions (Life Technologies). For isolation by adhesion, 1.5×10^8 to 2.5×10^8 PBMCs were transferred into culture flasks (175 cm²) containing 30 ml of standard culture medium (plus antibiotics) and kept under standard culture conditions for 2 hours to allow adherence of the monocytes to the flask surface. Next, growth medium was exchanged and cells were harvested after additional 24 hours of incubation in fresh medium (plus antibiotics). After isolation, cells were cultured in RPMI [10% fetal calf serum (FCS), no antibiotics] in 24-well plates [Costar Ultra-Low Cluster Plate (24-well); Corning Inc., 3473], with a density of 1×10^6 to 4×10^6 cells/ml and well. Purification and cell quality was determined by flow cytometry.

Immunoblotting

Twenty micrograms of protein was separated by 15 or 10% SDS-polyacrylamide gel electrophoresis and transferred onto nitrocellulose membranes. Primary antibody incubations were performed at 4°C overnight, blots were washed three times with PBS-T (PBS + 0.1% Tween 20). Secondary antibody was applied for 1 hour at room temperature. The blot was washed three times with PBS-T. Bands were detected with Pierce ECL Western Blotting Substrate (Thermo Scientific, 32209). Different exposure times were used depending on the primary antibody. To assess equal loading, blots were either cut or stripped and reprobed with an antibody recognizing glyceraldehyde-3-phosphate dehydrogenase (GAPDH). Primary antibodies used were as follows: STIM1 1:500, mouse, BD (610954); STIM2 1:2000, rabbit, Sigma (S8572); ORAI1 1:1000, Sigma (O8264); GAPDH 1:8000, rabbit, Santa Cruz (sc-25778). Secondary antibody was goat anti-rabbit [1:10000, Jackson ImmunoResearch (111-035-046)].

Bacterial strain and growth conditions

S. aureus cells were routinely grown on tryptic soy agar plates and in tryptic soy broth (Difco) in an orbital shaker set at 150 rpm and 37°C. For the monocyte phagocytosis and killing assay, liquid cultures of *S. aureus* strain SA113 (41) were grown to exponential growth phase (3 hours) and washed two times with PBS before usage.

siRNA-mediated protein knockdown

For knockdown studies, siRNA was introduced into the cells by nucleofection. Cells (7.5×10^6) were used per transfection and cultivated in RPMI 1640 medium + 10% FCS + glucose (2 g/liter) (without antibiotics). siRNA was purchased from Qiagen and Microsynth (ORAI1, ORAI2, ORAI3, and STIM1) and modified as previously described (24). STIM2 siRNA was from Microsynth and was used without further modification (table S1).

For control, pooled nonsilencing RNA (modified and unmodified) were used. ORAI1, ORAI2, ORAI3, and STIM1 siRNAs were used in a mixture 1:1, each 2 to 4 μl of a 20 μM stock solution and STIM2 with 2 to 4 μl of a 40 μM stock solution.

Fluorescence-based Ca^{2+} imaging

Measurements were performed as in (24). Shortly, the cells were loaded with 1 μM Fura-2 AM (in RPMI + 10% FCS + 10 mM Hepes) for 30 min, and measurements were performed in physiological Ringer's bath solution containing varying concentrations of free Ca^{2+} . SOCE was triggered using 1 μM thapsigargin or 1 μM fMLF.

Quantitative reverse transcription polymerase chain reaction

Total RNA was isolated from 1.5×10^6 cells, and qRT-PCR was performed using the QuantiTect SYBR Green Kit (Qiagen, 204145) (24, 42). RNA from BALF was isolated using the RNeasy Plus Micro Kit (Qiagen, 74034) following the manufacturer's protocol. RNA from mouse lung tissue (25 mg) was isolated on ice using the RNeasy Mini Kit (Qiagen, 74104) and deoxyribonuclease digest (Qiagen, 79254). RNA was transcribed with Omniscript RT Kit (Qiagen, 205111) and used for qRT-PCR.

Primer sequences used for detection are listed in tables S2 and S3. Positive controls for primer verification were generated by performing standard PCR on specific cDNA using the desired primers and further cloning of the received products into the pJET vector.

Fluorescence-based ROS measurements

Extracellular H_2O_2 production by monocytes was measured using the H_2O_2 -sensitive and H_2O_2 -specific fluorescent dye Amplex UltraRed (AUR) (Invitrogen, Molecular Probes, A36006), following the manufacturer's instructions. Assay component concentrations were 50 μM for AUR, 0.5 U/ml for horseradish peroxidase, and 100 U/ml for superoxide dismutase (SOD) (for sufficient conversion of $^{\cdot}\text{O}_2^-$ to H_2O_2). H_2O_2 production was triggered by thapsigargin, fMLF, and PMA (1 μM). Experiments were performed in 96-well plates (black/transparent) using the Tecan GENios Pro Reader with a bottom reading setting. All experiments were conducted in Ringer's solution (1 mM Ca^{2+}) with 25,000 cells per well as duplicates or triplicates. $[\text{H}_2\text{O}_2]_i$ was calculated from relative fluorescence units (RFU) after calibration of the system. Intracellular ROS was determined on a single-cell level by the fluorescent dye 5-(and-6)-carboxy-2,7-difluorodihydrofluorescein diacetate ($\text{H}_2\text{-DCFDA}$) (excitation 485 nm/emission 535 nm). Cells were loaded with $\text{H}_2\text{-DCFDA}$ (1 μM) for 30 min and imaged with a conventional fluorescence microscope.

EPR spectroscopy

Monocyte $^{\cdot}\text{O}_2^-$ production was performed with a Bruker spectrometer (ESP300e) equipped with a standard 4102ST cavity holding the capillary support quartz glass finger, and under standard conditions: temperature, 37°C (controller BioIII-TGC, Noxygen); modulation amplitude, 0.1 mT; microwave power, 20 mW. Spectra were recorded every 60 s to monitor kinetic behavior.

Monocytes were counted, and 250,000 or 500,000 cells were taken for experiments and stimulated in Ringer's buffer. For monitoring superoxide production, the redox-activated cyclic hydroxylamine spin trap CMH (1-hydroxy-3-methoxycarbonyl-2,2,5,5-tetramethylpyrrolidine) was added (300 μM), and the sample (50 μl in glass capillary) was immediately transferred into the capillary holder. The oxygen concentration of all solutions was $\sim 200 \mu\text{M}$. All control experiments with single components of the assays and CMH were tested for unwanted radical production. In addition, superoxide radical as the reacting species was identified by sup-

pression of the CMH signal by SOD (100 U/ml) as superoxide scavenger. The peak-to-peak intensities of the CM radical EPR spectra of the time series were evaluated with the homemade program Medea and compared to a reference sample of known concentration [usually 100 μM Tempol (4-hydroxy-2,2,6,6-tetramethylpiperidin-1-oxyl)] recorded under identical conditions for quantitative measures.

Bead phagocytosis

Fluoresbrite Yellow Green Microspheres (Polysciences GmbH) with a size of 1 μm were used for the analysis of the contribution of ORAI/STIM-mediated SOCE in monocyte phagocytosis. Monocytes (5×10^5) were used per condition and incubated with 1×10^7 beads (20 \times excess of beads) for 4 hours. The efficiency of phagocytosis was determined using flow cytometry (BD FACSCalibur flow cytometer, Becton-Dickinson). The monocyte population was gated on a dot plot graph. The percentage of fluorescent cells (indicating the uptake of beads) was determined in reference to the total number of gated cells.

Bacterial phagocytosis and killing assay

Monocytes were seeded in 12-well polystyrene plates (1×10^5 cells per well) in RPMI + 10% FCS and allowed to attach for 1 hour in a humidified atmosphere at 37°C and 5% CO_2 . Subsequently, monocytes were inoculated with PBS-washed SA113 cells at a multiplicity of infection of 10, centrifuged at 400g for 5 min to sediment the bacteria, and coincubated for 60 min. To kill extracellular bacteria, cultures were subsequently supplemented with 50 $\mu\text{g}/\text{ml}$ gentamicin (Refobacin, Merck) and incubated for an additional hour as described above. At the end of the incubation time, monocytes were harvested by scraping, transferred into an Eppendorf tube, and centrifuged at 1700g for 2 min. Supernatants were removed and tested for viable bacteria, and cell pellets were resuspended in H_2O . Subsequently, monocytes were lysed by sonication at 50 W for 15 s, and CFUs were determined by plating serial dilutions of the lysates on Mueller-Hinton agar (Becton-Dickinson). Plates were incubated for 24 hours at 37°C before colonies were counted.

Acute lung infection model

Animal experiments were approved by the Landesamt für Soziales, Gesundheit und Verbraucherschutz of the State of Saarland following the national guidelines for animal treatment. Nine-week-old female C57BL/6 mice were anesthetized by intraperitoneal injection and intranasally infected with 2.5×10^7 CFU of the low-passage human *S. aureus* isolate strain SA564 (43) and PBS, respectively. Six hours after the bacterial challenge, mice were euthanized, the tracheae were cannulated, and a bronchoalveolar lavage was performed with 1 ml of PBS flushed three times into the lungs. Lungs were subsequently removed, and the left lobes of the lungs were immediately snap-frozen in liquid nitrogen and stored at -80°C until usage for RNA isolation. The right lobes of the lung were homogenized in 1 ml of PBS and subsequently used for CFU determinations by plating out serial dilutions of the homogenates on tryptic soy agar plates supplemented with 5% sheep blood (BD) and incubating the plates for 24 hours at 37°C. A small aliquot of the BALF was removed for CFU determinations, and the remaining BALF was split and centrifuged at 300g and 4°C for 10 min to obtain BALF cells and cell-free supernatants. One-fifth of the BALF cells were suspended in 200 μl of PBS, and total cell numbers were determined by light microscopy using a Neubauer hemocytometer. The remaining parts of the cell pellet were snap-frozen in liquid nitrogen and stored at -80°C until usage for RNA isolation.

Data analysis and statistics

Data collection and analysis were done using Microsoft Excel. Origin 6.1 was used to calculate IC_{50} values, and qRT-PCR data were collected and

analyzed using the MX-3000 software or Bio-Rad CFX manager. Imaging data were recorded with TillvisION software. All data sets were tested for outliers using the Grubbs' test. Unless otherwise indicated, for statistical evaluation of the unpaired/paired, two-sided standard Student's *t* test was applied, and significance was indicated with **P* < 0.05, ***P* < 0.01, and ****P* < 0.001. All measurements and qRT-PCRs were performed with cells or samples from at least two different donors and transfections and three measurements or runs per condition.

SUPPLEMENTARY MATERIALS

www.sciencesignaling.org/cgi/content/full/9/418/ra26/DC1

Text S1. ORAI-NOX2 feedback loop: A theoretical model—Detailed description.

Fig. S1. ORAI, TRP, and NOX abundance in primary human monocytes.

Fig. S2. Transcript and Western blot analysis of ORAI1, STIM1, and STIM2 abundance in primary human monocytes.

Fig. S3. ORAI and STIM control monocyte oxidative burst.

Fig. S4. The role of ORAI1 in monocyte oxidative burst: Alternative statistical evaluation.

Fig. S5. The role of ORAI1, STIM1, and STIM2 in monocyte phagocytosis of uncoated latex beads.

Fig. S6. PMA induces increase in *ORAI3/ORAI1* ratio in primary human monocytes.

Fig. S7. Effect of *S. aureus* challenge on immune cell recruitment in an acute murine lung infection model.

Table S1. siRNA primers.

Table S2. Primers used to detect human *ORAI*, *STIM*, *NOX*, and *DUOX* transcripts and various controls.

Table S3. Mouse primers used for qRT-PCR.

REFERENCES AND NOTES

- N. V. Serbina, T. Jia, T. M. Hohl, E. G. Pamer, Monocyte-mediated defense against microbial pathogens. *Annu. Rev. Immunol.* **26**, 421–452 (2008).
- D. C. Dale, L. Boxer, W. C. Liles, The phagocytes: Neutrophils and monocytes. *Blood* **112**, 935–945 (2008).
- C. Shi, E. G. Pamer, Monocyte recruitment during infection and inflammation. *Nat. Rev. Immunol.* **11**, 762–774 (2011).
- Y. Imai, K. Kuba, G. G. Neely, R. Yaghubian-Malhami, T. Perkmann, G. van Loo, M. Ermolaeva, R. Veldhuizen, Y. H. C. Leung, H. Wang, H. Liu, Y. Sun, M. Pasparakis, M. Kopf, C. Mech, S. Bavari, J. S. M. Peiris, A. S. Slutsky, S. Akira, M. Hultqvist, R. Holmdahl, J. Nicholls, C. Jiang, C. J. Binder, J. M. Penninger, Identification of oxidative stress and Toll-like receptor 4 signaling as a key pathway of acute lung injury. *Cell* **133**, 235–249 (2008).
- E. Galkina, K. Ley, Immune and inflammatory mechanisms of atherosclerosis (*). *Annu. Rev. Immunol.* **27**, 165–197 (2009).
- A. C. Cave, A. C. Brewer, A. Narayanapanicker, R. Ray, D. J. Grieve, S. Walker, A. M. Shah, NADPH oxidases in cardiovascular health and disease. *Antioxid. Redox Signal.* **8**, 691–728 (2006).
- R. K. Gandhirajan, R. K. Gandhirajan, S. Meng, H. C. Chandramoorthy, K. Mallilankaraman, S. Mancarella, H. Gao, R. Razmpour, X.-F. Yang, S. R. Houser, J. Chen, W. J. Koch, H. Wang, J. Soboloff, D. L. Gill, M. Madesh, Blockade of NOX2 and STIM1 signaling limits lipopolysaccharide-induced vascular inflammation. *J. Clin. Invest.* **123**, 887–902 (2013).
- J. D. Lambeth, NOX enzymes and the biology of reactive oxygen. *Nat. Rev. Immunol.* **4**, 181–189 (2004).
- K. Bedard, K. H. Krause, The NOX family of ROS-generating NADPH oxidases: Physiology and pathophysiology. *Physiol. Rev.* **87**, 245–313 (2007).
- M. Fahrmer, M. Muik, I. Derler, R. Schindl, R. Fritsch, I. Frischauf, C. Romanin, Mechanistic view on domains mediating STIM1–Orai coupling. *Immunol. Rev.* **231**, 99–112 (2009).
- P. G. Hogan, R. S. Lewis, A. Rao, Molecular basis of calcium signaling in lymphocytes: STIM and ORAI. *Annu. Rev. Immunol.* **28**, 491–533 (2010).
- J. Soboloff, M. A. Spassova, M. A. Dziadek, D. L. Gill, Calcium signals mediated by STIM and Orai proteins—A new paradigm in inter-organelle communication. *Biochim. Biophys. Acta* **1763**, 1161–1168 (2006).
- A. B. Parekh, J. W. Putney Jr., Store-operated calcium channels. *Physiol. Rev.* **85**, 757–810 (2005).
- M. Hoth, R. Penner, Depletion of intracellular calcium stores activates a calcium current in mast cells. *Nature* **355**, 353 (1992).
- P. Nunes, D. Comut, V. Bochet, U. Hasler, M. Oh-Hora, J.-M. Waldburger, N. Demaurex, STIM1 juxtaposes ER to phagosomes, generating Ca²⁺ hotspots that boost phagocytosis. *Curr. Biol.* **22**, 1990–1997 (2012).
- S. Brécard, S. Plançon, C. Melchior, E. J. Tschirhart, STIM1 but not STIM2 is an essential regulator of Ca²⁺ influx-mediated NADPH oxidase activity in neutrophil-like HL-60 cells. *Biochem. Pharmacol.* **78**, 504–513 (2009).
- N. Steinckwich, V. Schenten, C. Melchior, S. Brécard, E. J. Tschirhart, An essential role of STIM1, Orai1, and S100A8–A9 proteins for Ca²⁺ signaling and FcγR-mediated phagosomal oxidative activity. *J. Immunol.* **186**, 2182–2191 (2011).
- H. Zhang, R. A. Clemens, F. Liu, Y. Hu, Y. Baba, P. Theodore, T. Kurosaki, C. A. Lowell, STIM1 calcium sensor is required for activation of the phagocyte oxidase during inflammation and host defense. *Blood* **123**, 2238–2249 (2014).
- S. Brécard, C. Melchior, S. Plançon, V. Schenten, E. J. Tschirhart, Store-operated Ca²⁺ channels formed by TRPC1, TRPC6 and Orai1 and non-store-operated channels formed by TRPC3 are involved in the regulation of NADPH oxidase in HL-60 granulocytes. *Cell Calcium* **44**, 492–506 (2008).
- S. Yamamoto, S. Shimizu, S. Kiyonaka, N. Takahashi, T. Wajima, Y. Hara, T. Negoro, T. Hiroi, Y. Kiuchi, T. Okada, S. Kaneko, I. Lange, A. Fleig, R. Penner, M. Nishi, H. Takeshima, Y. Mori, TRPM2-mediated Ca²⁺ influx induces chemokine production in monocytes that aggravates inflammatory neutrophil infiltration. *Nat. Med.* **14**, 738–747 (2008).
- T. M. Link, U. Park, B. M. Vonakis, D. M. Raben, M. J. Soloski, M. J. Caterina, TRPV2 has a pivotal role in macrophage particle binding and phagocytosis. *Nat. Immunol.* **11**, 232–239 (2010).
- I. Bogeski, B. A. Niemeyer, Redox regulation of ion channels. *Antioxid. Redox Signal.* **21**, 859–862 (2014).
- I. Bogeski, R. Kappl, C. Kummerow, R. Gulaboski, M. Hoth, B. A. Niemeyer, Redox regulation of calcium ion channels: Chemical and physiological aspects. *Cell Calcium* **50**, 407–423 (2011).
- I. Bogeski, C. Kummerow, D. Al-Ansary, E. C. Schwarz, R. Koehler, D. Kozai, N. Takahashi, C. Peinelt, D. Griesemer, M. Bozem, Y. Mori, M. Hoth, B. A. Niemeyer, Differential redox regulation of ORAI ion channels: A mechanism to tune cellular calcium signaling. *Sci. Signal.* **3**, ra24 (2010).
- D. Prins, J. Groenendyk, N. Touret, M. Michalak, Modulation of STIM1 and capacitative Ca²⁺ entry by the endoplasmic reticulum luminal oxidoreductase ERp57. *EMBO Rep.* **12**, 1182–1188 (2011).
- B. J. Hawkins, K. M. Irmink, K. Mallilankaraman, Y.-C. Lien, Y. Wang, C. D. Bhanumathy, R. Subbiah, M. F. Ritchie, J. Soboloff, Y. Baba, T. Kurosaki, S. K. Joseph, D. L. Gill, M. Madesh, S-glutathionylation activates STIM, alters mitochondrial homeostasis. *J. Cell Biol.* **190**, 391–405 (2010).
- P. T. Mungai, G. B. Waypa, A. Jairaman, M. Prakriya, D. Dovic, M. K. Ball, P. T. Schumacker, Hypoxia triggers AMPK activation through reactive oxygen species-mediated activation of calcium release-activated calcium channels. *Mol. Cell. Biol.* **31**, 3531–3545 (2011).
- D. Alansary, I. Bogeski, B. A. Niemeyer, Facilitation of Orai3 targeting and store-operated function by Orai1. *Biochim. Biophys. Acta* **1853**, 1541–1550 (2015).
- P. Nunes, N. Demaurex, The role of calcium signaling in phagocytosis. *J. Leukoc. Biol.* **88**, 57–68 (2010).
- B. Bufe, T. Schumann, R. Kappl, I. Bogeski, C. Kummerow, M. Podgórska, S. Smola, M. Hoth, F. Zufall, Recognition of bacterial signal peptides by mammalian formyl peptide receptors: A new mechanism for sensing pathogens. *J. Biol. Chem.* **290**, 7369–7387 (2015).
- R. D. Ye, F. Boulay, J. M. Wang, C. Dahlgren, C. Gerard, M. Parmentier, C. N. Serhan, P. M. Murphy, International Union of Basic and Clinical Pharmacology. LXXIII. Nomenclature for the formyl peptide receptor (FPR) family. *Pharmacol. Rev.* **61**, 119–161 (2009).
- L.-J. Wu, T.-B. Sweet, D. E. Clapham, International Union of Basic and Clinical Pharmacology. LXXVI. Current progress in the mammalian TRP ion channel family. *Pharmacol. Rev.* **62**, 381–404 (2010).
- B. A. Miller, W. Zhang, TRP channels as mediators of oxidative stress. *Adv. Exp. Med. Biol.* **704**, 531–544 (2011).
- R. A. Clemens, C. A. Lowell, Store-operated calcium signaling in neutrophils. *J. Leukoc. Biol.* **98**, 497–502 (2015).
- R. Foyouzi-Youssefi, F. Petersson, D. P. Lew, K.-H. Krause, O. Nüsse, Chemoattractant-induced respiratory burst: Increases in cytosolic Ca²⁺ concentrations are essential and synergize with a kinetically distinct second signal. *Biochemical Journal* **322**, 709–718 (1997).
- S. Brécard, E. J. Tschirhart, Regulation of superoxide production in neutrophils: Role of calcium influx. *J. Leukoc. Biol.* **84**, 1223–1237 (2008).
- O. Nüsse, L. Serrander, R. Foyouzi-Youssefi, A. Monod, D. P. Lew, K.-H. Krause, Store-operated Ca²⁺ influx and stimulation of exocytosis in HL-60 granulocytes. *J. Biol. Chem.* **272**, 28360–28367 (1997).
- B. H. Segal, T. L. Leto, J. I. Gallin, H. L. Malech, S. M. Holland, Genetic, biochemical, and clinical features of chronic granulomatous disease. *Medicine* **79**, 170–200 (2000).
- S. Feske, CRAC channelopathies. *Pflugers Arch.* **460**, 417–435 (2010).
- S. Feske, ORAI1 and STIM1 deficiency in human and mice: Roles of store-operated Ca²⁺ entry in the immune system and beyond. *Immunol. Rev.* **231**, 189–209 (2009).

RESEARCH ARTICLE

41. S. Iordanescu, M. Surdeanu, Two restriction and modification systems in *Staphylococcus aureus* NCTC8325. *J. Gen. Microbiol.* **96**, 277–281 (1976).
42. A. S. Wenning, K. Neblung, B. Strauss, M. J. Wolfs, A. Sappok, M. Hoth, E. C. Schwarz, TRP expression pattern and the functional importance of TRPC3 in primary human T-cells. *Biochim. Biophys. Acta* **1813**, 412–423 (2011).
43. G. A. Somerville, M. S. Chaussee, C. I. Morgan, J. R. Fitzgerald, D. W. Dorward, L. J. Reitzer, J. M. Musser, *Staphylococcus aureus* aconitase inactivation unexpectedly inhibits post-exponential-phase growth and enhances stationary-phase survival. *Infect. Immun.* **70**, 6373–6382 (2002).

Acknowledgments: We are grateful to A. Stark, S. Janku, B. Strauss, C. Hässig, and G. Schwär for their technical assistance. We thank the Clinical Hemostaseology and Transfusion Medicine, Saarland University (H. Eichler) for providing LRS chambers for PBMC isolation. We also thank M. Hoth for his continuous support. **Funding:** This work is supported by the Medical Faculty of Saarland (HOMFOR excellent research grant to I.B. and HOMFOR research grant to E.C.S. and H.S.) and by the DFG (Deutsche Forschungsgemeinschaft): SFB1027 project A1 to H.R., B2 to M.H., and C4 to I.B. and B.A.N., and BO3643/3-1 research grant (to I.B.). **Author contributions:** S.S., B.A.N., and I.B. designed

the study. The mathematical model was designed, calculated, and written by H.R. with the help of B.S. S.S., C.S.G., A.L., B.P., D.C., P.J., R.G., B.W., and E.D. performed experiments. S.S., C.S.G., A.L., H.S., T.V., E.C.S., M.B., M.H., T.T., B.A.N., and R.K. supervised experiments and/or analyzed the data. I.B. wrote the manuscript with the help of S.S. **Competing interests:** The authors declare that they have no competing interests. **Data and materials availability:** There are no material transfer agreements or restrictions. All data and materials are freely available.

Submitted 29 December 2015

Accepted 22 February 2016

Final Publication 8 March 2016

10.1126/scisignal.aaf1639

Citation: S. Saul, C. S. Gibhardt, B. Schmidt, A. Lis, B. Pasiaka, D. Conrad, P. Jung, R. Gaupp, B. Wonnemberg, E. Diler, H. Stanisz, T. Vogt, E. C. Schwarz, M. Bischoff, M. Herrmann, T. Tschernig, R. Kappl, H. Rieger, B. A. Niemeyer, I. Bogeski, A calcium-redox feedback loop controls human monocyte immune responses: The role of ORAI Ca²⁺ channels. *Sci. Signal.* **9**, ra26 (2016).

A calcium-redox feedback loop controls human monocyte immune responses: The role of ORAI Ca²⁺ channels

Stephanie Saul, Christine S. Gibhardt, Barbara Schmidt, Annette Lis, Bastian Pasieka, David Conrad, Philipp Jung, Rosmarie Gaupp, Bodo Wonneberg, Ebru Diler, Hedwig Stanisz, Thomas Vogt, Eva C. Schwarz, Markus Bischoff, Mathias Herrmann, Thomas Tschernig, Reinhard Kappl, Heiko Rieger, Barbara A. Niemeyer and Ivan Bogeski (March 8, 2016)
Science Signaling **9** (418), ra26. [doi: 10.1126/scisignal.aaf1639]

The following resources related to this article are available online at <http://stke.sciencemag.org>.
This information is current as of March 9, 2016.

Article Tools	Visit the online version of this article to access the personalization and article tools: http://stke.sciencemag.org/content/9/418/ra26
Supplemental Materials	" <i>Supplementary Materials</i> " http://stke.sciencemag.org/content/suppl/2016/03/04/9.418.ra26.DC1
Related Content	The editors suggest related resources on <i>Science's</i> sites: http://stke.sciencemag.org/content/sigtrans/3/115/ra24.full http://stke.sciencemag.org/content/sigtrans/8/407/ra128.full http://stke.sciencemag.org/content http://stke.sciencemag.org/content/sigtrans/9/418/pc6.full
References	This article cites 43 articles, 18 of which you can access for free at: http://stke.sciencemag.org/content/9/418/ra26#BIBL
Permissions	Obtain information about reproducing this article: http://www.sciencemag.org/about/permissions.dtl

Science Signaling (ISSN 1937-9145) is published weekly, except the last December, by the American Association for the Advancement of Science, 1200 New York Avenue, NW, Washington, DC 20005. Copyright 2016 by the American Association for the Advancement of Science; all rights reserved.